Cross-Linking and Amyloid Formation by N- and C-Terminal Cysteine Derivatives of Human Apolipoprotein C-II†

Chi L. L. Pham,‡ Danny M. Hatters,‡ Lynne J. Lawrence,§ and Geoffrey J. Howlett*,‡

Russell Grimwade School of Biochemistry and Molecular Biology, The University of Melbourne, Parkville, Victoria 3010, Australia, and CSIRO Health Sciences and Nutrition, 343 Royal Parade, Parkville, Victoria 3052, Australia

Received May 3, 2002; Revised Manuscript Received July 22, 2002

ABSTRACT: We have investigated the effect of disulfide cross-linking on amyloid formation by human apolipoprotein (apo) C-II. Three derivatives of apoC-II were generated by inserting a cysteine residue on either the N-terminus (C_N-apoC-II), C-terminus (C_C-apoC-II), or both termini (C_NC_C-apoC-II). Under reducing conditions, all derivatives formed amyloid with a fibrous ribbon morphology similar to that of wild-type apoC-II. Under oxidizing conditions, C_N- and C_NC_C-apoC-II formed a highly tangled network of fibrils, suggesting that the addition of an N-terminal cysteine to apoC-II promotes interfibril disulfide cross-links. Fibrils formed by C_C-apoC-II under oxidizing conditions were closely packed but less tangled than fibrils formed by the C_N and C_NC_C derivatives. The frequency of closed ring structures was more than doubled for C_C-apoC-II compared to wild-type apoC-II. The kinetics of fibril formation by all cysteine derivatives was markedly enhanced under oxidizing conditions, suggesting that disulfide cross-linking promotes amyloid formation. Substoichiometric levels of preformed C_N- and C_C-apoC-II dimers accelerate amyloid formation by wild-type apoC-II. These data suggest that the N- and C-termini of apoC-II are close together in the amyloid fibril such that covalent cross-linking of either the N or C end of apoC-II promotes nucleation and the "seeding" of fibril growth.

Amyloid fibrils are long fibrous protein polymers associated with a number of human diseases including Alzheimer's, Parkinson's, and Creutzfeldt−Jakob. Common properties of these fibrils include a cable or ribbonlike morphology and a rich content of cross β-structure (*1*, *2*). While the amino acid sequences of amyloid-forming proteins share no sequence similarity or other obvious patterns, many have partially unfolded molten globule-like tertiary structures that correlate with their ability to form amyloid (*3*−*5*). For example, a mutant of cystatin C (L68Q) that is associated with cerebral amyloid angiopathy is more vulnerable to proteolysis in cultured media and aggregates more extensively in vitro than the wild-type protein (*6*, *7*). The observation that many unrelated peptide sequences form amyloid under non-native conditions leads to the idea that most, if not all, proteins can form amyloid and that evolutionary pressure selects for proteins that fold rapidly and cooperatively to avoid partially folded states and the amyloidogenic pathway (*3*, *8*). However, posttranslational events can influence the folding process. For example, a transthyretin derivative, vulnerable to amyloid formation in the monomeric state, is protected from amyloid formation by forming heterocomplexes with another mutant that stabilizes the tetramer over monomer (*9*). Lipid-free human plasma apolipoprotein (apo)[1] C-II slowly forms amyloid ribbons (*10*), whereas in the presence of phospholipid, apoC-II has α-helical structure and amyloid formation is inhibited (*11*−*13*). ApoC-II appears to be typical of other apolipoproteins with a predisposition to form amyloid (*14*−*20*). Apolipoproteins associated with amyloid deposition in vivo, including apoA-I (*14*, *15*), apoA-II (*16*, *17*), apoA-IV (*18*), and apoE (*19*, *20*), are mostly truncated (*14*, *16*, *19*, *20*), suggesting that proteolysis may promote unfolding and the amyloidogenic folding pathway (*13*).

Amyloid formation involves an initial rate-limiting nucleation step followed by rapid elongation and recruitment of monomers to form fibrils (*21*, *22*). A number of studies indicate that amyloidosis can be accelerated by "seeding" with preformed amyloid (*23*−*25*). Prion proteins in mammals (*26*) and yeast (*27*, *28*) self-propagate by seeding where infectivity is perpetuated by the recruitment of normally folded monomers onto the amyloid polymer. In the case of fibril formation by tau, dimerization via disulfide linkage is a prerequisite for nucleation (*25*). Disulfide bond formation also plays a role in amyloid formation by a number of other proteins such as the prion protein (*29*, *30*) and the ABri protein associated with familial British dementia (*31*). In each case, oxidation of cysteine residues to form disulfide bonds within these proteins enhances amyloid formation (*25*, *29*, *31*).

We have investigated the effects of disulfide cross-linking on amyloid formation by apoC-II. Naturally occurring apoC-II has no cysteine residues. Adding cysteine residues to either

† This work was funded by grants from the National Health and Medical Research Council of Australia to G.J.H., and D.M.H. was a recipient of a Melbourne Research Scholarship.

* Corresponding author. Tel: 61-3-8344-7632. Fax: 61-3-9347-7730. E-mail: ghowlett@unimelb.edu.au.

‡ The University of Melbourne.

§ CSIRO Health Sciences and Nutrition.

[1] Abbreviations: apo, apolipoprotein; SDS, sodium dodecyl sulfate; GuHCl, guanidine hydrochloride; CD, circular dichroism.

10.1021/bi026070v CCC: $22.00
Published on Web 10/25/2002

Table 1: Primer Sequences Used for Generating ApoC-II Cysteine Derivatives of cDNA[a]

primer	direction of primer	sequence[a,b]
apoC-II F	forward	5′ CATATGACCCAACAGCCCCAGCAAGATG
apoC-II R	reverse	5′ *GGATCC*TTACTCCTCTCCCTTCAGCACAG
C_N-apoC-II F	forward	5′ CATATG**TGT**ACCCAACAGCCCCAGCAAGATG
C_C-apoC-II R	reverse	5′ *GGATCC*TTA**ACA**CTCCTCTCCCTTCAGCACAG

[a] *Bam*HI (underlined and italicized) and *Nde*I (underlined) restriction sites are shown. [b] The new cysteine codons are shown in bold.

the N-terminus (C_N-apoC-II), C-terminus (C_C-apoC-II), or both termini (C_NC_C-apoC-II) of apoC-II accelerates amyloid formation under oxidizing conditions. Substoichiometric levels of preformed covalently linked dimers accelerate amyloid formation by wild-type apoC-II, highlighting the potential impact of oxidative cross-linking on the rate of amyloid formation by proteins in vivo.

MATERIALS AND METHODS

Materials. Oligonucleotide primers were purchased from GibcoBRL Life Technologies (Sydney, NSW, Australia). Restriction endonucleases, Vent DNA polymerase, and T4 DNA ligase were obtained from New England Biolabs (Beverley, MA). Taq DNA polymerase was purchased from Boehringer Mannheim (Castle Hill, NSW, Australia). The pGEM-T vector and *Escherichia coli* JM109 high-efficiency competent cells were purchased from Promega (Annandale, NSW, Australia). pET11a expression vector and the *E. coli* BL21(DE3) expression host were purchased from Novagen (Madison, WI). A western blot kit and polyclonal antibodies to apoC-II were purchased from Calbiochem (Kilsyth, VIC, Australia).

In Vitro Mutagenesis of ApoC-II cDNA. Forward and reverse PCR primers were designed to incorporate an extra cysteine codon at either the N- or C-terminus of the cDNA sequence encoding mature apoC-II. These primers also were designed to encode a *Bam*HI or *Nde*I restriction site to allow directional cloning (Table 1). The modified DNA was generated through PCR amplification from a cDNA clone generously provided by Dr. N. Schachter (*32*). After the PCR, the DNA was subcloned into the pGEM-T vector and then into pET11a via the *Nde*I and *Bam*HI restriction sites (which are incorporated into pGEM by the primers) according to standard procedures (*33*). The modified DNA sequences were verified by sequencing (ABI Prism BigDye Terminator Cycle Sequencing Ready Reaction Kits, Perkin-Elmer Biosystems, Wellesley, MA).

Expression and Purification of ApoC-II and the Cysteine Derivatives. Wild-type apoC-II was expressed and purified as described previously (*10*, *34*). For the apoC-II cysteine derivatives, identical procedures were used except the buffer for gel filtration was at pH 6.8 and contained 10 mM DTT. After elution from the anion-exchange column, the apoC-II cysteine derivatives were exhaustively dialyzed against 10 mM ammonium bicarbonate, pH 8.0, at 4 °C. The samples were lyophilized and stored in 5 M GuHCl, 10 mM DTT, and 10 mM Tris-HCl, pH 8.0, at −20 °C. The concentrations of all proteins were determined using an extinction coefficient of 12090 M^{-1} cm^{-1} based on amino acid composition (*35*).

Tris−Tricine SDS−PAGE and Western Blots. Samples were analyzed by 16.5% T, 3% C, Tris−Tricine SDS−PAGE as described (*36*) under either reducing (+100 mM DTT in the loading sample) or nonreducing conditions (no DTT). For direct Coomassie Blue visualization of the proteins, the gels were stained using 0.1% (w/v) Coomassie Blue R-250 for 5 h and destained using 30% (v/v) methanol and 10% (v/v) acetic acid. For western blot analysis, proteins were electrophoretically transferred from gels to Protran nitrocellulose membranes (Schleicher and Schuell, Dassell, Germany), and the membranes were blocked using 5% (w/v) skim milk powder. Rabbit anti-human apoC-II (Calbiochem) was used for primary immunobinding at a dilution of 1/1000. Goat anti-rabbit IgG, conjugated to peroxidase (Calbiochem), was used as a secondary antibody with a working dilution of 1/10000. Samples were visualized by colorimetric detection using TMB (3,3′,5,5′-tetramethylbenzidine) solution (Calbiochem).

Amyloid Formation. Unfolded proteins (10−17 mg/mL) in 5 M GuHCl, 10 mM DTT, and 10 mM Tris-HCl, pH 8.0, were directly diluted in refolding buffer (100 mM sodium phosphate, pH 7.4, and 0.1% sodium azide) to a final concentration of 0.3 mg/mL. The turbidity of freshly prepared protein in refolding buffer (2 mL) at a concentration of 0.3 mg/mL was monitored at a wavelength of 400 nm at 20 °C (Cary-5 spectrophotometer; Varian, Clayton, Australia). The samples were covered with sealing film to avoid evaporation.

Congo Red binding assays were performed using protein samples (150 μg/mL) in refolding buffer with or without 2.5 μM Congo Red. Samples were incubated for 5 min at room temperature before absorption spectra (400−600 nm) were measured using either a Cary-5 spectrophotometer (Varian, Clayton, Australia) or a λ-2 spectrometer (Perkin-Elmer). Absorption spectra were also measured for Congo Red alone in refolding buffer in the presence and absence of 10 mM DTT. The scattering contribution of the proteins (from spectra of protein samples in the absence of Congo Red) was deducted from the relevant Congo Red spectra.

Thioflavin T reactivity assays were performed by adding aliquots of 30−100 μL of apoC-II in refolding buffer (0.3 mg/mL) to the wells of a microtiter plate containing refolding buffer and 5 μM thioflavin T to a total volume of 300 μL. Samples were incubated for 5 min prior to measurement of fluorescence intensities using an f_{max} fluorescence plate reader (Molecular Devices, Sunnyvale, CA) equipped with excitation and emission filters of 444 and 485 nm, respectively. Measurements were performed in triplicate.

Transmission Electron Microscopy. Copper or gold grids (400 mesh) were coated with thin carbon film and glow discharged in nitrogen. Samples of apoC-II (0.3 mg/mL) in refolding buffer were diluted to a concentration of 0.1 mg/mL with Tris-buffered saline (137 mM NaCl, 3 mM KCl, 25 mM Tris-HCl, pH 7.4). The diluted samples were applied to the grids for 2 min within 15 min of glow discharging and washed twice with Tris-buffered saline, followed by staining with 3−4 drops of 2% potassium phosphotungstate at pH 6.0−7.0 or 2% uranyl acetate. The grids were air-

dried and examined using a JEOL 2000FX transmission electron microscope (Brooksvale, NSW, Australia) operating at 120 kV. Micrographs were recorded at nominal magnifications of 15000× and 40000×.

Formation of Disulfide-Linked Dimers. Denatured samples of C_N- and C_C-apoC-II (17 and 11 mg/mL, respectively) containing 10 mM DTT were dialyzed into 5 M GuHCl, 10 mM Tris-HCl, pH 8.0 at 4 °C, with three buffer changes over 2 days. The samples were incubated in the presence of air for approximately 1 week at room temperature.

Analytical Ultracentrifugation. Samples of apoC-II/cysteine derivatives (380 μL), preincubated for 72 h at 20 °C, were analyzed at 20 °C using the XL-A analytical ultracentrifuge (Beckman/Coulter, Fullerton, CA). Samples were subjected to centrifugation at a rotor speed of 5000 rpm, and radial scans were measured using a wavelength of 280 nm at 10 min intervals. Data were collected using 0.002 cm radial increments in the continuous scanning mode. Data were analyzed using ls-g*(s) analysis (*37*) with the baseline absorbance set to zero and sedimentation range from 1 to 1500 S and 100 sedimentation coefficient increments. A regularization parameter of $p = 0.95$ was used.

RESULTS

Expression and Purification of ApoC-II Cysteine Derivatives. Expression of the apoC-II mutants (C_N-, C_C-, and C_CC_N-apoC-II) in *E. coli* was comparable to that typically observed for wild-type apoC-II in that the induced proteins localized to *E. coli* inclusion bodies (*34*). We therefore used a similar purification procedure for the apoC-II cysteine derivatives but maintained reducing conditions during the gel filtration step by adding 10 mM DTT to the buffer. Electrophoretic analysis of the expressed proteins after anion-exchange chromatography shows prominent bands of the expected molecular mass of approximately 9 kDa (Figure 1A). Western blot analysis of the samples using antibodies to apoC-II indicated strong immunoreactivity associated with the major species in Figure 1A ($M_r = 9$ kDa) but not the minor higher molecular mass band (between 14.4 and 21 kDa) observed in the C_N- and C_NC_C-apoC-II samples (data not shown). Yields between 8 and 12 mg of protein/L of bacterial culture were routinely obtained with purities of approximately 90−95% based on SDS−PAGE analysis. This contrasts to typical yields of approximately 15 mg/L for wild-type apoC-II (*10*).

Amyloid Formation by ApoC-II Cysteine Derivatives. We employed turbidity (*38*) to monitor aggregation of the apoC-II cysteine derivatives under reducing (+10 mM DTT; Figure 2A) and oxidizing conditions (no DTT; Figure 2B). The turbidity profiles presented in Figure 2 are representative of the results of three separate experiments. Under reducing conditions, wild-type apoC-II shows a gradual change in turbidity similar to our previous observations (*10*, *12*, *38*). The change in turbidity of the C_N- and C_C-apoC-II derivatives under these conditions is comparable to wild-type apoC-II. However, for the C_NC_C-apoC-II derivative, aggregation is more rapid over the same time scale, showing a further 70% increase in turbidity after 80 h of incubation. These results contrast with the behavior observed under oxidizing conditions, where the apoC-II cysteine derivatives develop turbidity more rapidly than wild-type apoC-II. C_N-apoC-II shows

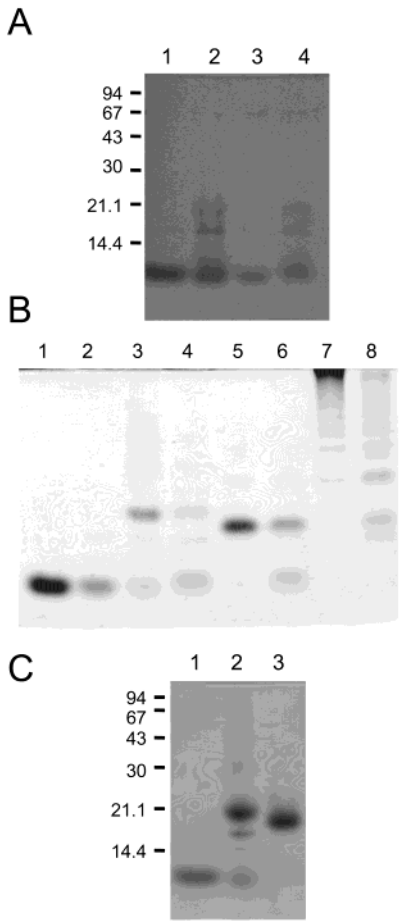

FIGURE 1: Tris−Tricine SDS−PAGE analysis of apoC-II cysteine derivatives. Molecular mass markers (kDa) are indicated to the left of the gels. (A) Reducing gel of protein collected after purification by anion-exchange chromatography. Lanes: 1, wild-type apoC-II; 2, C_N-apoC-II; 3, C_C-apoC-II; 4, C_NC_C-apoC-II. (B) Nonreducing gel of freshly prepared apoC-II cysteine derivatives (0.3 mg/mL protein in refolding buffer) incubated for 82 h in the presence (lanes 2, 4, 6, and 8) and absence (lanes 1, 3, 5, and 7) of 10 mM DTT. Lanes: 1 and 2, wild-type apoC-II; 3 and 4, C_N-apoC-II; 5 and 6, C_C-apoC-II; 7 and 8, C_NC_C-apoC-II. (C) Nonreducing gel of air-oxidized apoC-II cysteine derivatives (incubated for 1 week in 5 M GuHCl, no DTT). Lanes: 1, wild-type apoC-II; 2, C_N-apoC-II; 3, C_C-apoC-II.

a sigmoidal increase in turbidity after a gradual rise during the first 10 h. The change in turbidity of the C_C-apoC-II sample shows a lag phase similar to that of wild-type apoC-II for the first 24 h followed by a rapid increase in turbidity to a new plateau level. The C_NC_C-apoC-II derivative produced the most rapid and extensive turbidity increase accompanied by an unusual drop in turbidity after incubation for 40 h that we attribute to visible settling of the material. This drop in the turbidity was not observed for an identical sample that was stirred (Figure 2B, solid circles).

At the conclusion of the turbidity assays, samples were analyzed by Tris−Tricine SDS−PAGE under nonreducing conditions to assess the extent of disulfide formation. In the presence of SDS, wild-type apoC-II aggregates resolve as a single band (Figure 1B, lanes 1 and 2). The aggregates formed by C_N- and C_C-apoC-II under oxidizing conditions show a prominent band corresponding approximately to the mobility of dimer (Figure 1B, lanes 3 and 5). The C_N- and C_C-apoC-II derivatives incubated in the presence of DTT show a lower proportion of this higher molecular mass band

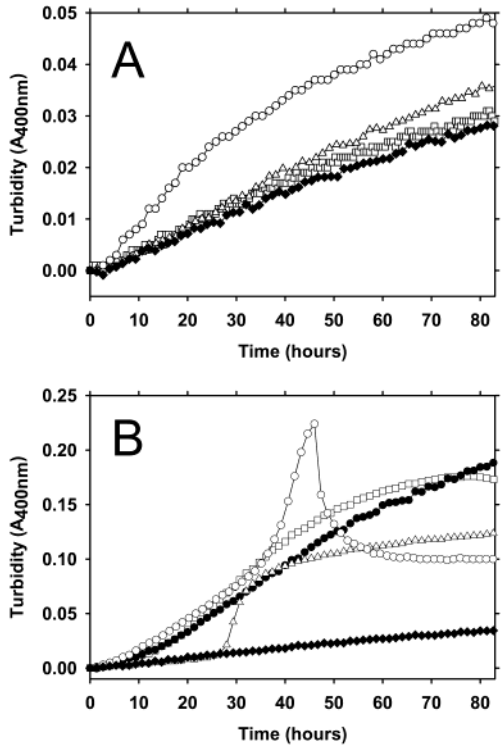

FIGURE 2: Time-dependent turbidity of the apoC-II cysteine derivatives. Freshly prepared samples (0.3 mg/mL protein in refolding buffer) were incubated at 20 °C in the presence (panel A) and absence (panel B) of 10 mM DTT. Turbidity was monitored by absorbance at 400 nm. Samples shown are wild-type apoC-II (◆), C_N-apoC-II (□), C_C-apoC-II (△), C_NC_C-apoC-II (○), and C_NC_C-apoC-II stirred using a magnetic stirrer (●).

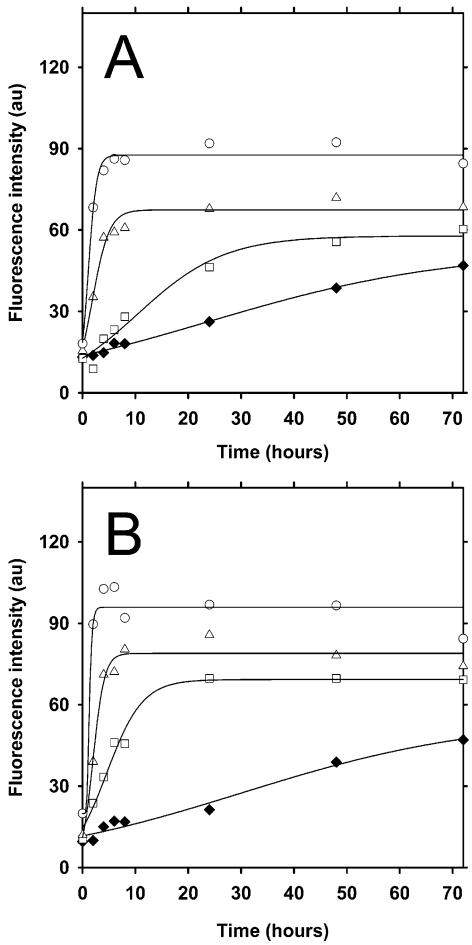

FIGURE 3: Thioflavin T reactivity of apoC-II cysteine derivatives. Freshly prepared samples (0.3 mg/mL protein in refolding buffer) were incubated at 20 °C in the presence (panel A) and absence (panel B) of 10 mM DTT. Thioflavin T reactivity was measured using 100 μL sample aliquots and a fluorescence plate reader with excitation and emission filters of 444 and 485 nm, respectively. Samples shown are wild-type apoC-II (◆), C_N-apoC-II (□), C_C-apoC-II (△), and C_NC_C-apoC-II (○).

(Figure 1B, lanes 4 and 6). We attribute the difference between the mobility of the putative C_N- and C_C-apoC-II dimers (M_r = 21 and 18 kDa, respectively) to an anomaly due to the complex association of these cross-linked apoC-II cysteine derivatives with SDS micelles. For the C_NC_C-apoC-II, under both reducing and oxidizing conditions, a series of higher molecular mass oligomers with negligible monomer are observed (Figure 1B, lanes 7 and 8). Western blot analysis shows that all of the oxidation-induced higher molecular mass bands in Figure 1B have significant anti-apoC-II immunoreactivity (data not shown). These results suggest that disulfide formation accompanies aggregation by the cysteine-containing apoC-II derivatives.

A defining characteristic of apoC-II amyloid fibrils is the capacity to induce changes in the fluorescence properties of thioflavin T (*10*). We therefore used thioflavin T reactivity to measure the rate of amyloid formation by the apoC-II cysteine derivatives (Figure 3). In all cases the initial rate of amyloid formation was faster for the cysteine-containing derivatives under oxidizing conditions (Figure 3B) compared to reducing conditions (Figure 3A). These results support the conclusion drawn from Figures 1 and 2 that oxidizing conditions promote the aggregation of the cysteine-containing apoC-II derivatives. Comparison of the time courses in Figures 2 and 3 indicates that the rise in thioflavin T reactivity precedes the increase in turbidity, suggesting that these two measurements reflect different properties of the amyloid fibrils.

The aggregates formed by the cysteine derivatives were tested for Congo Red reactivity as another indicator of the presence of amyloid. The spectrum of Congo Red alone shows a maximum absorbance at a wavelength of 490 nm. The addition of freshly prepared wild-type apoC-II causes a small change in the wavelength maximum and a small increase in the absorbance, whereas the addition of aged apoC-II results in a significant increase in absorbance and a shift in the wavelength maximum to approximately 510 nm (Figure 4A) (*10*, *38*). The presence of 10 mM DTT had no effect on the absorption spectrum of Congo Red in the presence of freshly prepared wild-type apoC-II or of wild-type apoC-II incubated for 4 days (Figure 4B). Each of the apoC-II cysteine derivatives was tested for Congo Red reactivity under both reducing and oxidizing conditions (Figure 4C−H). Freshly prepared samples (0.3 mg/mL) had similar effects on the Congo Red absorption spectrum compared to freshly prepared wild-type apoC-II. Samples incubated for 4 days, under either oxidizing or reducing conditions, produced changes in the Congo Red absorption spectrum similar to those observed for wild-type apoC-II amyloid incubated under identical conditions.

We next investigated the morphologies of the apoC-II cysteine derivatives using negative staining transmission electron microscopy. The aggregates formed by wild-type

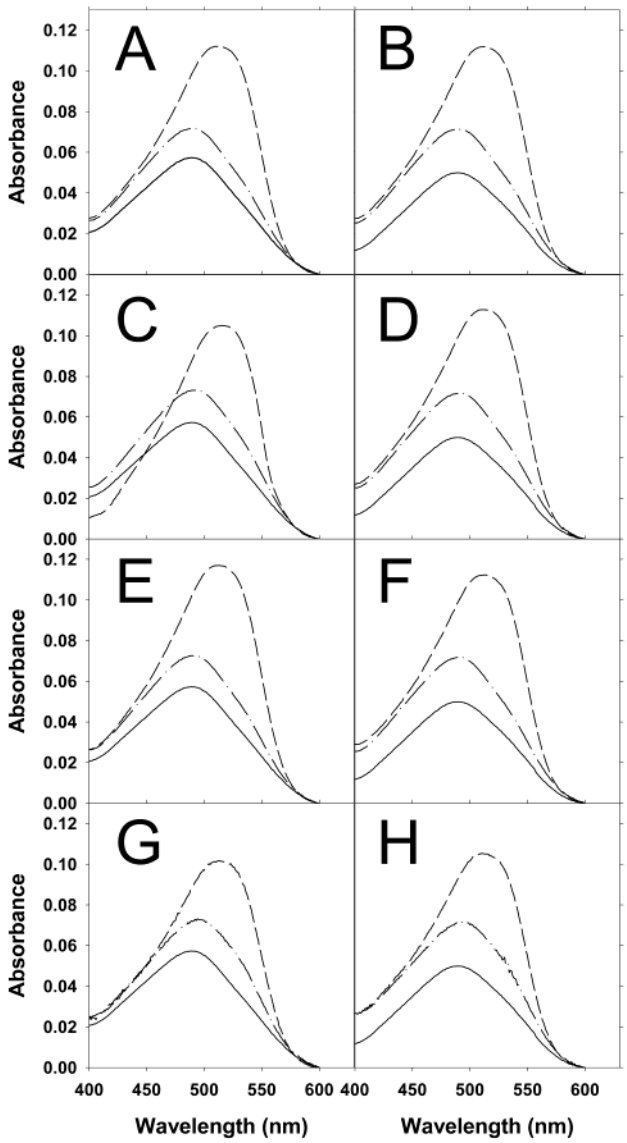

FIGURE 4: Interaction of Congo Red with apoC-II cysteine derivatives. Wild-type apoC-II and cysteine derivatives (150 μg/mL) freshly prepared (dashed−dotted lines) and incubated for 4 days (dashed lines) were mixed with 2.5 μM Congo Red, and absorption spectra were determined. The solid lines refer to the spectra of 2.5 μM Congo Red alone. Samples were prepared in the absence of DTT (panels A, C, E, and G for wild-type apoC-II, C_N-apoC-II, C_C-apoC-II, and C_NC_C-apoC-II, respectively) and presence of 10 mM DTT (panels B, D, F, and H for wild-type apoC-II, C_N-apoC-II, C_C-apoC-II, and C_NC_C-apoC-II, respectively).

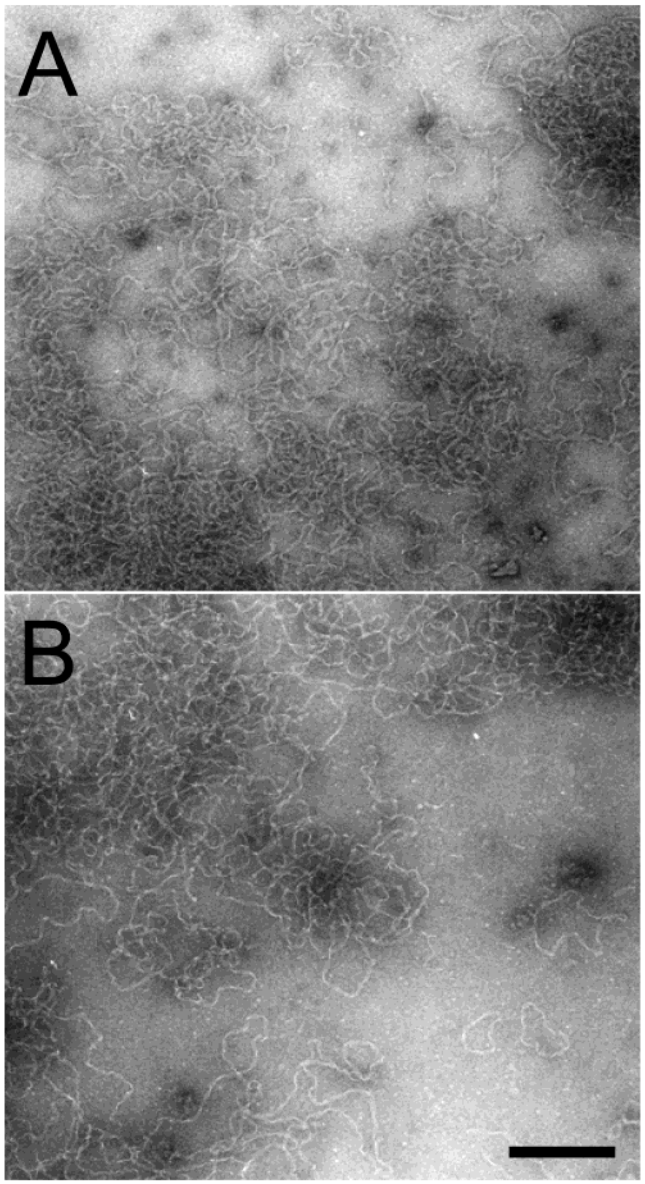

FIGURE 5: Transmission electron micrographs of wild-type apoC-II amyloid fibrils formed in the presence (A) and absence (B) of 10 mM DTT. Scale bar = 200 nm.

apoC-II in the presence or absence of 10 mM DTT (Figure 5) have morphologies similar to those previously observed, consisting of twisted ribbonlike fibrils with a number of closed loop structures (*10*). Under reducing conditions, C_N-apoC-II forms amyloid with a morphology similar to that of wild-type apoC-II (Figure 6A). However, the morphology changes dramatically when aggregates of C_N-apoC-II form under oxidizing conditions (Figure 6B). The fibrils are more tangled and matted than those formed under reducing conditions. This may explain the more rapid increase in turbidity of the C_N-apoC-II under oxidizing conditions (Figure 2B) since these patches of matted fibrils could scatter more light than individual fibrils. C_C-apoC-II forms fibrils in the presence of 10 mM DTT with a morphology similar to that of wild-type apoC-II (Figure 7A). Under oxidizing conditions, C_C-apoC-II forms patches of matted fibrils (Figure 7B), although to lesser extent than for the other apoC-II cysteine derivatives. Of note is an apparent increase for the frequency of closed loop formation compared with wild-type apoC-II. Analysis of this observation involved counting the number of loops present in 10 micrographs of random electron microscopy fields containing oxidized C_C-apoC-II or wild-type apoC-II. The average number of closed loops in randomly selected fields (at a nominal magnification of 15000×) was 87 closed loops per field for oxidized C_C-apoC-II compared to 35 for wild-type apoC-II with standard deviations of 33 and 10, respectively. Figure 8A shows the morphology of the amyloid formed by C_NC_C-apoC-II under reducing conditions. The fibrils are more tangled compared to wild-type apoC-II and the other cysteine-containing apoC-II derivatives in a similar environment, perhaps accounting for the increase in the time-dependent changes in turbidity (Figure 2A). When C_NC_C-apoC-II is incubated under oxidizing conditions, the morphology of the fibrils is similar to

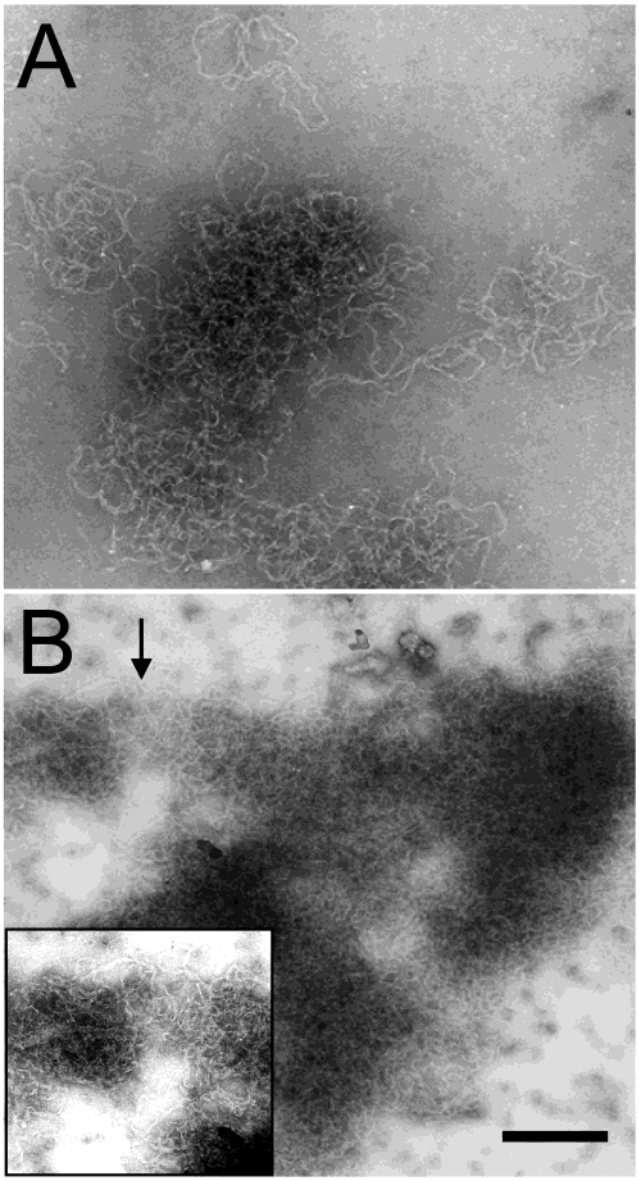

FIGURE 6: Transmission electron micrographs of C_N-apoC-II amyloid fibrils formed in the presence (A) and absence (B) of 10 mM DTT. Scale bar = 200 nm. The inset in panel B represents an enlargement of a section within the micrograph (arrow).

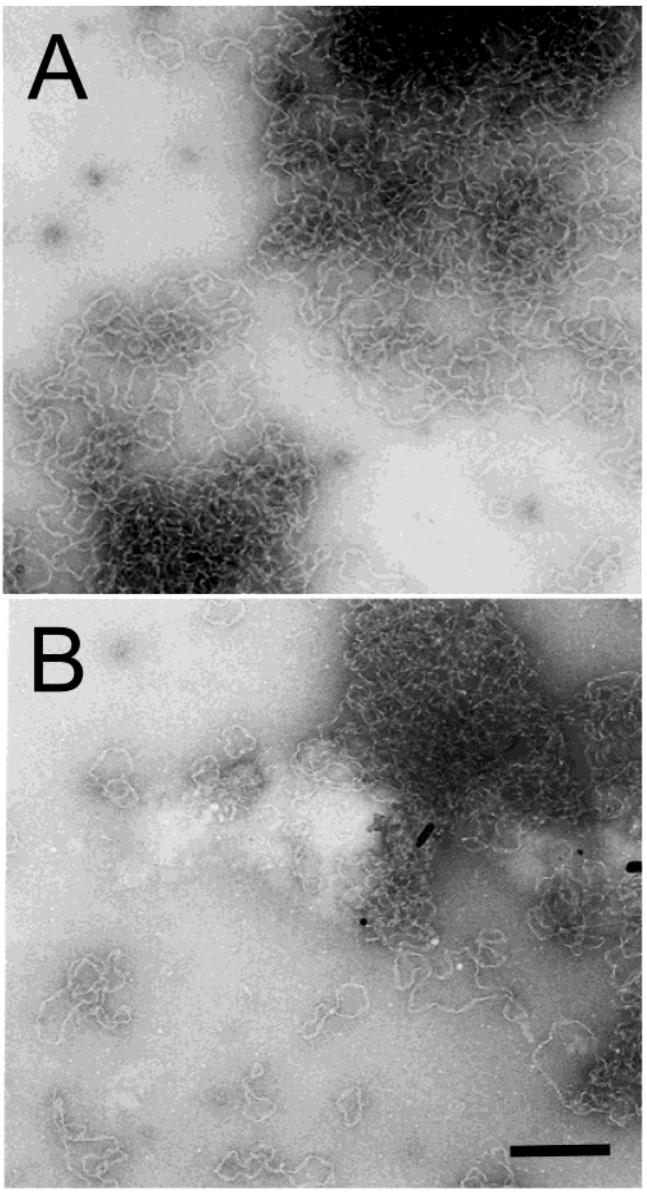

FIGURE 7: Transmission electron micrographs of C_C-apoC-II amyloid fibrils formed in the presence (A) and absence (B) of 10 mM DTT. Scale bar = 200 nm.

that observed for the C_N-apoC-II (Figure 8B) with patches of fibrils that are extensively tangled and entwined. This network formation would account for the rapid increase in the turbidity (Figure 2B). Settling of these large masses of fibril would also explain the large drop in the turbidity after 40 h in nonstirred samples (Figure 2B).

Seeding Wild-Type ApoC-II Amyloid Formation with Disulfide-Linked Dimers. The role of disulfide cross-linking in amyloid formation was further investigated using cross-linked dimers to "seed" amyloid formation by wild-type apoC-II. The dimeric species were prepared by air oxidation of C_N- and C_C-apoC-II samples in 5 M GuHCl and 10 mM Tris-HCl, pH 8.0. Nonreducing Tris−Tricine SDS−PAGE analysis showed that, after 1 week of air oxidation at room temperature, 90%−100% of each protein is dimeric (Figure 1C).

Turbidity analysis shows that the preformed, covalently linked, C_N-apoC-II dimer alone aggregates more rapidly compared with wild-type apoC-II over 72 h (Figure 9A). The addition of increasing quantities of C_N-apoC-II dimer to a fixed total concentration of wild-type apoC-II results in systematic increases in the rates of turbidity development (Figure 9A). This suggests that preformed C_N-apoC-II dimers promote apoC-II fibril formation. Incubation of preformed, covalently linked, C_C-apoC-II dimer alone produces much higher turbidity than either preformed C_N-apoC-II dimer alone or wild-type apoC-II (Figure 9B). Addition of C_C-apoC-II dimer to wild-type apoC-II results in systematic rises in the turbidity time course as the proportion of C_C-apoC-II is increased.

The significant differences in turbidity of wild-type apoC-II and the apoC-II cysteine-containing derivatives may be due to the different morphologies of the amyloid fibrils formed under oxidizing conditions (Figures 5−8). To more directly monitor amyloid fibril formation, we used thioflavin T reactivity as a quantitative method to follow amyloid formation. Our previous studies indicate that thioflavin T reactivity is proportional to the concentration of wild-type

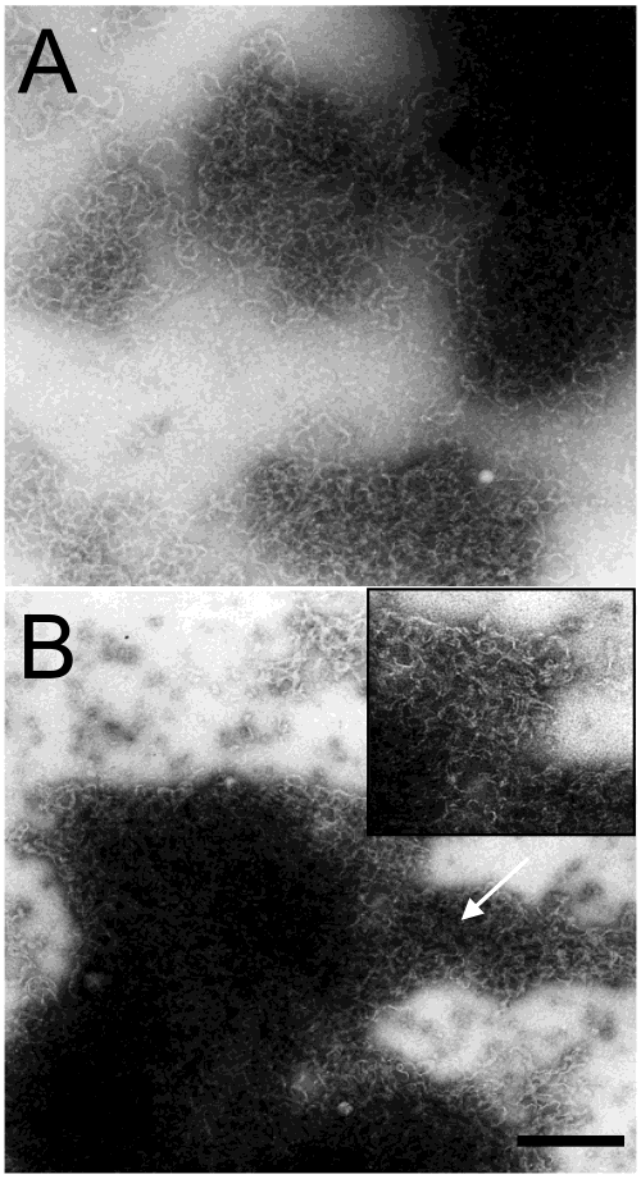

FIGURE 8: Transmission electron micrographs of C_NC_C-apoC-II amyloid fibrils formed in the presence (A) and absence (B) of 10 mM DTT. Scale bar = 200 nm. The inset in panel B represents an enlargement of a section within the micrograph (arrow).

apoC-II amyloid fibrils (*38*). Wild-type apoC-II alone shows a gradual rise in the accumulation of thioflavin T reactive material over 72 h (Figure 10). In contrast, the C_N-apoC-II dimer (Figure 10A) and C_C-apoC-II dimer (Figure 10B) alone produce more rapid development of thioflavin T reactivity. For instance, C_N-apoC-II dimer alone reaches an apparent maximum thioflavin T reactivity after 20 h incubation, while C_C-apoC-II dimer alone develops maximum thioflavin T reactivity in less than 10 h incubation. The addition of either C_N- or C_C-apoC-II dimer at a substoichiometric subunit molar ratio of 10:1, wild-type apoC-II to dimer, is sufficient to increase the overall rate of amyloid formation close to that observed by each dimer alone. On increasing the stoichiometry of wild-type apoC-II to dimer, the kinetics of amyloid formation systematically approach that of wild-type apoC-II alone. Compared to C_N-apoC-II dimer (Figure 10A), lower amounts of C_C-apoC-II dimer (Figure 10B) are required to enhance wild-type apoC-II amyloid formation.

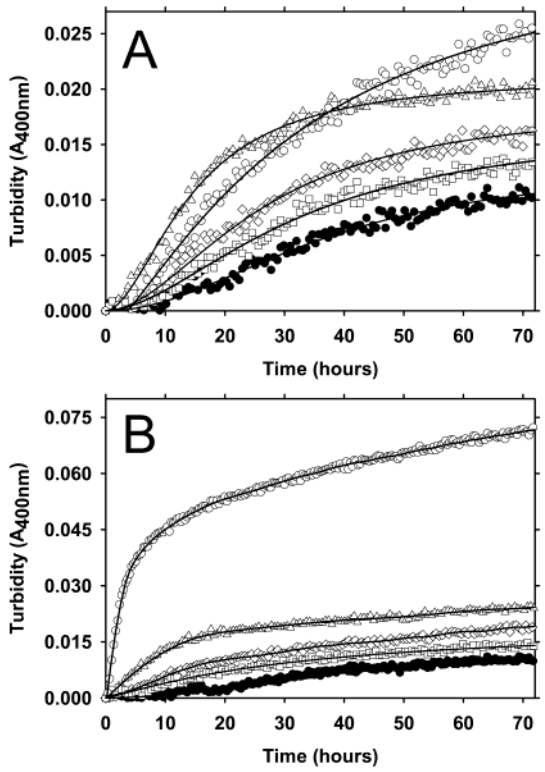

FIGURE 9: Time-dependent turbidity of wild-type apoC-II seeded with preformed disulfide-linked dimers of C_N- (A) and C_C-apoC-II (B). Total protein concentrations are 0.3 mg/mL with samples incubated at 20 °C. Samples shown include C_N- or C_C-apoC-II dimers alone (○), wild-type apoC-II alone (●), and mixtures containing molar ratios of wild-type apoC-II to disulfide-linked dimers of 100:1 (□), 50:1 (◇), and 10:1 (△).

The samples present after the incubations shown in Figure 10 were further examined by sedimentation velocity analysis. Figure 11 shows sedimentation coefficient distributions obtained by fitting the data assuming a distribution of nondiffusing particles (*37*). This model gave excellent fits to the sedimentation scans. Analysis of wild-type apoC-II aggregates (open triangles) produced a narrow sedimentation coefficient distribution (20−200 S) with a mode of approximately 100 S, consistent with our previous studies (*10*, *12*, *38*). In contrast, sedimentation analysis of incubated cross-linked C_N-apoC-II dimer alone produced a much broader sedimentation coefficient distribution (20−900 S) and a less clearly resolved mode of approximately 150 S (Figure 11A). The sedimentation coefficient distributions of aggregates formed by a mixture of wild-type apoC-II and cross-linked C_N-apoC-II dimer are more similar to wild-type apoC-II. The sedimentation coefficient distribution modes for the mixtures at ratios of 10:1 and 100:1 wild-type apoC-II to C_N-apoC-II dimer are approximately 150 and 120 S, respectively, with much narrower ranges of values (between 20 and 500 S and 20−350 S, respectively; Figure 11A) compared to C_N-apoC-II dimer alone. Aggregates formed by cross-linked C_C-apoC-II dimer alone produced fits with a broad sedimentation coefficient distribution (approximately 20−1200 S; Figure 11B). The sedimentation coefficient distributions for aggregates containing 10:1 and 100:1 wild-type apoC-II to cross-linked C_C-apoC-II dimer were similar to wild-type apoC-II with modes of approximately 150 S and ranges of 20−350 S.

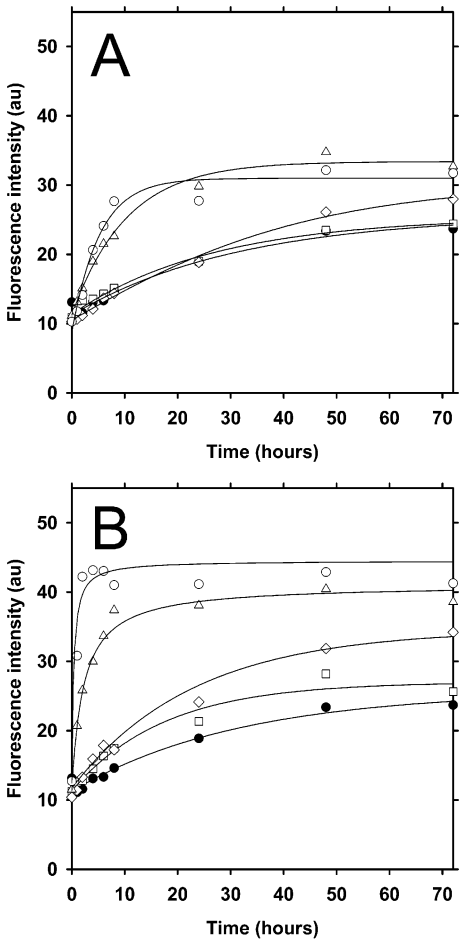

FIGURE 10: Time-dependent thioflavin T reactivity of wild-type apoC-II seeded with preformed dimers of C_N- (A) and C_C-apoC-II (B). Total protein concentrations are 0.3 mg/mL with samples incubated at 20 °C, and thioflavin T reactivity was measured using 30 μL sample aliquots. Samples shown include C_N- or C_C-apoC-II dimers alone (○), wild-type apoC-II alone (●), and mixtures containing molar ratios of wild-type apoC-II to disulfide-linked dimers of 100:1 (□), 50:1 (◇), and 10:1 (△).

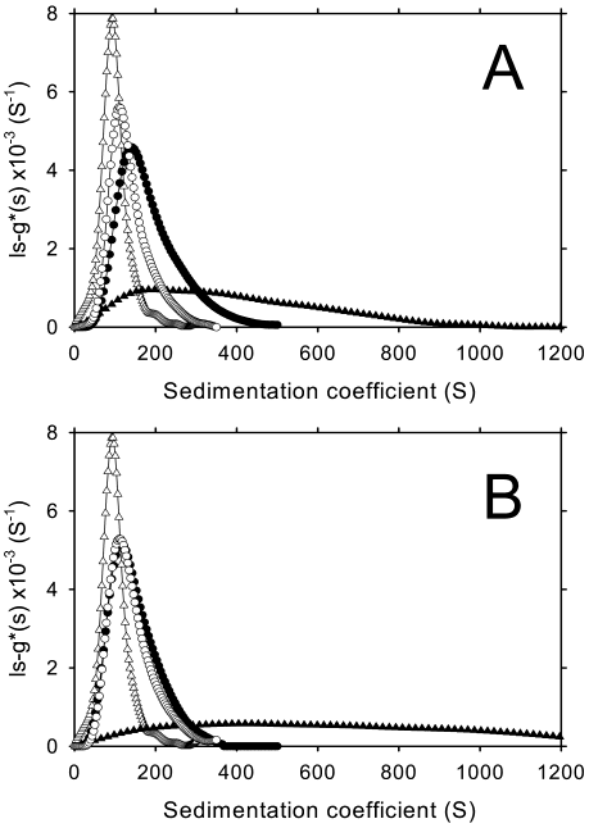

FIGURE 11: Sedimentation coefficient distributions of wild-type apoC-II amyloid fibrils seeded with preformed dimers of C_N- (A) and C_C-apoC-II (B). The sedimentation velocity profiles (5000 rpm, 20 °C) of fibrils formed by incubation for 72 h were fitted to sedimentation coefficient distributions (*37*). The fitted distributions are shown of C_N- or C_C-apoC-II dimers alone (▲), wild-type apoC-II alone (△), and mixtures containing molar ratios of wild-type apoC-II to disulfide-linked dimers of 100:1 (○) and 10:1 (●).

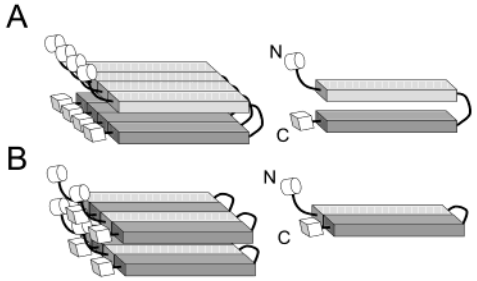

FIGURE 12: Models of the apoC-II amyloid structure. In these models, the fibril is a ribbon comprised of two parallel layers of β-sheet (left), formed by the stacking of apoC-II molecules folded into β-hairpins (right). The β-strands of the apoC-II molecules are represented as solid blocks (N-terminal β-strand indicated in light gray and C-terminal β-strand in dark gray). Additional cysteine residues are shown as cylinders and cubes at the N- and C-termini, respectively. (A) In this model, the β-strands of one apoC-II molecule stack in both β-sheets. (B) In this alternative model, both β-strands of each apoC-II monomer stack consecutively within one β-sheet.

DISCUSSION

During amyloidosis under oxidizing conditions the cysteine-containing apoC-II derivatives form fibrils more rapidly and become extensively tangled compared to wild-type apoC-II (Figures 5−8). We interpret these results using the alternate models for amyloid assembly presented in Figure 12. These models incorporate the measured width of apoC-II amyloid ribbons (13 nm), determined from negative staining electron microscopy studies (*10*), and average thickness of 2 nm, determined using atomic force microscopy (unpublished results). A simple way to fit the apoC-II amino acid sequence into this geometry is to assume a double β-sheet core and to fold the 79 residues into a β-hairpin generating a theoretical β-strand length of approximately 12.5 nm. It is important to note that a β-strand of this length is long compared to strands observed in globular proteins and that the model could be modified to allow for two or more discontinuous strands along the fibril width. The proposed stacking pattern of β-strands, perpendicular to the long fibril axis, is similar to a model developed for the amyloid assembly of the SH3 domain (*40*). The putative β-hairpins could assemble into β-sheets in several ways, and Figure 12 presents just two plausible models. In Figure 12A, each β-hairpin provides a strand in each of the two β-sheets. Alternatively, in Figure 12B, each β-hairpin provides two consecutive strands within one β-sheet. Both of these stacking arrangements (Figure 12, panels A and B) are consistent with the results in this study, where the additional cysteine residues at the N- or C-terminus (Figure 12, shown as cylinders and cubes) are

located on one side of the fibril in close proximity. This would explain disulfide linkage during amyloid formation (Figure 1) and the stimulation of amyloid formation by preformed dimers of C_C- or C_N-apoC-II (Figures 9 and 10). The substoichiometric subunit concentrations of preformed dimers to wild-type apoC-II (1:10) required to promote amyloidosis (Figures 9 and 10) indicate that preformed disulfide-linked dimers seed amyloid formation by wild-type apoC-II. Of note is the ability of the C_C-apoC-II dimers alone to form amyloid more rapidly than the C_N-apoC-II dimers alone (Figure 10). This suggests that cross-linking apoC-II at the C-terminus provides a better seed for amyloid assembly than cross-linking at the N-terminus. The models shown in Figure 12 incorporate a flexible region that extends from the N-terminus of the β-hairpin. This is to account for the observation that apoC-II derivatives containing an N-terminal cysteine form highly tangled networks (Figures 6 and 8), suggesting that the N-terminus is more extended from the amyloid core structure to allow interfibril cross-linking. In addition, the first 12 N-terminal residues of apoC-II contain 3 proline residues, suggesting local structural heterogeneity and a reduced likelihood of β-strand formation.

The influence of disulfide cross-links on the kinetics of amyloid formation can be compared to other amyloid systems. For the prion protein, disulfide cross-linkages are important in stabilizing the normal cellular α-helical conformation, since reducing conditions at low pH promote interconversion into soluble β-rich monomers that are thought to resemble the pathogenic conformation (*40*). Other groups have suggested that thiol−disulfide interchange between the α-helical monomer and the β-rich polymer plays an important role in promoting fibril growth and providing resistance to proteolysis and depolymerization (*29*, *30*). In these schemes, the close proximity of thiol and disulfide groups of the α-helical monomer and β-rich polymer favors a disulfide-free thiol interchange that results in intermolecular disulfide links and a conformational change from α-helix into the β-rich pathogenic conformation (*29*, *30*). In the case of the ABri protein (*31*), intramolecular cross-links promote a conformation that is more susceptible to amyloid formation. Disulfide dimerization of tau protein is a prerequisite for nucleation (*25*). The ability of disulfide formation to stabilize oligomers raises the prospect that disulfide formation in vivo plays a critical role in amyloidosis.

Posttranslational events that affect amyloid formation, such as protein truncation and covalent oligomerization, may also directly affect processes that regulate amyloid formation. In our recent studies, we have proposed that chaperones play an important regulatory role in the inhibition of amyloid formation in vivo (*41*, *42*). While chaperones are conventionally considered to assist with the folding of partially unfolded globular proteins during protein synthesis, we found two chaperones associated with amyloid deposits (α-crystallin and clusterin) that inhibit apoC-II amyloid formation at substoichiometric concentrations (*41*, *42*). The substoichiometric level of inhibition (∼1:100 molar ratio, chaperone to apoC-II) suggests a specific interaction between the chaperone and the amyloidogenic nuclei, preventing its progression into amyloid fibrils by promoting its dissociation back to monomers (*41*, *42*). In the event of covalent cross-linking of the amyloidogenic nuclei, this mechanism for chaperone activity would be rendered ineffective. Covalent cross-linking of amyloidogenic nuclei could circumvent such regulatory processes in vivo.

Oxidative stress is associated with a number of pathologies, notably advanced atherosclerosis (*43*) and Alzheimer's disease (*44*). Oxidative modification induced by free radicals can also result in covalent cross-linking, such as dityrosine formation (*43*). Insoluble α-synuclein from brain amyloid lesions, oxidatively modified with 3-nitrotyrosine derivatives, also forms covalently linked oligomers (*45*, *46*). In vitro nitration of α-synuclein promotes O−O′ dityrosine cross-linking and stabilizes preformed α-synuclein fibrils from urea-induced dissociation (*47*). The ability of preformed covalently linked dimers of apoC-II to accelerate amyloid formation of wild-type apoC-II at substoichiometric concentrations sheds light on the nucleation-dependent pathway and suggests that factors that promote covalent dimerization of amyloidogenic proteins have the ability to substantially accelerate their rate of amyloid formation.

REFERENCES

1. Sunde, M., and Blake, C. C. (1998) *Q. Rev. Biophys. 31*, 1−39.
2. Dobson, C. M. (1999) *Trends Biochem. Sci. 24*, 329−332.
3. Dobson, C. M. (2001) *Biochem. Soc. Symp. 68*, 1−26.
4. Nettleton, E. J., Sunde, M., Lai, Z., Kelly, J. W., Dobson, C. M., and Robinson, C. V. (1998) *J. Mol. Biol. 281*, 553−564.
5. Booth, D. R., Sunde, M., Bellotti, V., Robinson, C. V., Hutchinson, W. L., Fraser, P. E., Hawkins, P. N., Dobson, C. M., Radford, S. E., Blake, C. C., and Pepys, M. B. (1997) *Nature 385*, 787−793.
6. Wei, L., Berman, Y., Castano, E. M., Cadene, M., Beavis, R. C., Devi, L., and Levy, E. (1998) *J. Biol. Chem. 273*, 11806−11814.
7. Abrahamson, M., and Grubb, A. (1994) *Proc. Natl. Acad. Sci. U.S.A. 91*, 1416−1420.
8. Lansbury, P. T. (1999) *Proc. Natl. Acad. Sci. U.S.A. 96*, 3342−3344.
9. Hammarstrom, P., Schneider, F., and Kelly, J. W. (2001) *Science 293*, 2459−2462.
10. Hatters, D. M., MacPhee, C. E., Lawrence, L. J., Sawyer, W. H., and Howlett, G. J. (2000) *Biochemistry 39*, 8276−8283.
11. MacRaild, C. A., Hatters, D. M., Howlett, G. J., and Gooley, P. R. (2001) *Biochemistry 40*, 5414−5421.
12. Hatters, D. M., Lawrence, L. J., and Howlett, G. J. (2001) *FEBS Lett. 494*, 220−224.
13. Hatters, D. M., and Howlett, G. J. (2002) *Eur. Biophys. J. 31*, 2−8.
14. Westermark, P., Mucchiano, G., Marthin, T., Johnson, K. H., and Sletten, K. (1995) *Am. J. Pathol. 147*, 1186−1192.
15. Wisniewski, T., Golabek, A. A., Kida, E., Wisniewski, K. E., and Frangione, B. (1995) *Am. J. Pathol. 147*, 238−244.
16. Higuchi, K., Kitagawa, K., Naiki, H., Hanada, K., Hosokawa, M., and Takeda, T. (1991) *Biochem. J. 279*, 427−433.
17. Benson, M. D., Liepnieks, J. J., Yazaki, M., Yamashita, T., Hamidi Asl, K., Guenther, B., and Kluve-Beckerman, B. (2001) *Genomics 72*, 272−277.
18. Bergstrom, J., Murphy, C., Eulitz, M., Weiss, D. T., Westermark, G. T., Solomon, A., and Westermark, P. (2001) *Biochem. Biophys. Res. Commun. 285*, 903−908.
19. Wisniewski, T., Lalowski, M., Golabek, A., Vogel, T., and Frangione, B. (1995) *Lancet 345*, 956−958.
20. Huang, Y., Liu, X. Q., Wyss-Coray, T., Brecht, W. J., Sanan, D. A., and Mahley, R. W. (2001) *Proc. Natl. Acad. Sci. U.S.A. 98*, 8838−8843.
21. Harper J. D., and Lansbury P. T. (1997) *Annu. Rev. Biochem. 66*, 385−407.
22. Ferrone, F. (1999) *Methods Enzymol. 309*, 256−274.
23. Wood, S. J., Wypych, J., Steavenson, S., Louis, J.-C., Citron, M., and Biere, A. L. (1999) *J. Biol. Chem. 274*, 19509−19512.
24. Kayed, R., Bernhagen, J., Greenfield, N., Sweimeh, K., Brunner, H., Voelter, W., and Kapurniotu, A. (1999) *J. Mol. Biol. 287*, 781−796.
25. Friedhoff, P., Bergen, M. V., Mandelkow, E.-M., Davies, P., and Mandelkow, E. (1998) *Proc. Natl. Acad. Sci. U.S.A. 95*, 15712−15717.

26. Prusiner, S. B. (1998) *Proc. Natl. Acad. Sci. U.S.A. 95*, 13363−13383.
27. Lindquist, S. (1997) *Cell 89*, 495−498.
28. Osherovich, L. Z., and Weissman, J. S. (2002) *Dev. Cell 2*, 143−151.
29. Welker, E., Wedemeyer, W. J., and Scheraga, H. A. (2001) *Proc. Natl. Acad. Sci. U.S.A. 98*, 4334−4336.
30. Feughelman, M., and Willis, B. K. (2000) *J. Theor. Biol. 206*, 313−315.
31. El-Agnaf, O. M. A., Sheridan, J. M., Sidera, C., Siligardi, G., Hussain, R., Haris, P. I., and Austen, B. M. (2001) *Biochemistry 40*, 3449−3457.
32. Jackson, C. L., Bruns, G. A. P., and Breslow, J. L. (1984) *Proc. Natl. Acad. Sci. U.S.A. 81*, 2945−2949.
33. Sambrook, J., Fritsch, E. F., and Maniatis, T. (1989) *Molecular Cloning: A Laboratory Manual*, 2nd ed., Cold Spring Harbor Laboratory Press, Cold Spring Harbor, NY.
34. Wang, C. S., Downs, D., Dashti, A., and Jackson, K. W. (1996) *Biochim. Biophys. Acta 1302*, 224−230.
35. Edelhoch, H. (1967) *Biochemistry 8*, 1948−1954.
36. Schagger, H., and von Jagow, G. (1987) *Anal. Biochem. 166*, 368−379.
37. Schuck, P., and Rossmanith, P. (2000) *Biopolymers 54*, 328−341.
38. Hatters, D. M., Minton, A. P., and Howlett, G. J. (2002) *J. Biol. Chem. 277*, 7824−7830.
39. Jimenez, J. L., Guijarro, J. I., Orlova, E., Zurdo, J., Dobson, C. M., Sunde, M., and Saibil, H. R. (1999) *EMBO J. 18*, 815−821.
40. Jackson, G. S., Hosszu, L. L., Power, A., Hill, A. F., Kenney, J., Saibil, H., Craven, C. J., Waltho, J. P., Clarke, A. R., and Collinge, J. (1999) *Science 283*, 1935−1937.
41. Hatters, D. M., Linder, R. A., Carver, J. A., and Howlett, G. J. (2001) *J. Biol. Chem. 276*, 33755−33761.
42. Hatters, D. M., Wilson, M. R., Easterbrook-Smith, S. B., and Howlett, G. J. (2002) *Eur. J. Biochem. 269*, 2789−2794.
43. Dean, R. T., Fu, S., Stocker, R., and Davies, M. J. (1997) *Biochem. J. 324*, 1−18.
44. Smith, M. A., Rottkamp, C. A., Nunomura, A., Raina, A. K., and Perry, G. (2000) *Biochim. Biophys. Acta 1502*, 139−144.
45. Giasson, B. I., Duda, J. E., Murray, I. V., Chen, Q., Souza, J. M., Hurtig, H. I., Ischiropoulos, H., Trojanowski, J. Q., and Lee, V. M. (2000) *Science 290*, 985−989.
46. Baba, M., Nakajo, S., Tu, P. H., Tomita, T., Nakaya, K., Lee, V. M., Trojanowski, J. Q., and Iwatsubo, T. (1998) *Am. J. Pathol. 152*, 879−884.
47. Souza, J. M., Giasson, B. I., Chen, Q., Lee, V. M., and Ischiropoulos, H. (2000) *J. Biol. Chem. 275*, 18344−18349.

BI026070V